GENERATION AND CALIBRATION OF HIGH RESOLUTION DEM FROM SINGLE BASELINE SPACEBORNE INTERFEROMETRY: THE 'SPLIT-SWATH' APPROACH

Davide Giudici[1], Andrea Monti Guarnieri[2], Daniele Mapelli[1], and Fabio Rocca[2]

[1]*ARESYS SRL, Via Bistolfi 49, 20134, Milan, Italy, Email: info@aresys.it*
[2]*Politecnico di Milano - DEI, Via Ponzio 34/5,20133, Milan, Italy, Email:monti@elet.polimi.it*

ABSTRACT

The paper is focused on the main limits to the performances of the DEM retrieval from SAR interferometry, measured in terms of horizontal resolution and vertical accuracy. A mathematical model is developed to assess the accuracy of the location in 3D, given the two SAR images and a set of calibrated references, or Ground Control Point, with known accuracy, whereas we assume that the geometry of the interferometer, say the baselines, are known only at a very rough approximation. Simplified relations, used to compute the expected DEM retrieval accuracy, are derived and it is found that a two non-adjacent sub-swaths approach (the 'split-swath' approach) improves the calibration efficiency. A numerical example, referring to a Ka-band single-pass interferometer, is also presented.

Key words: Interferometry; SAR; DEM.

1. INTRODUCTION

The generation of Digital Elevation Models (DEMs) through single pass SAR interferometry is one of the most important applications of the SAR systems, particularly spaceborne, for the large coverage that can be achieved and the relatively short time to generate global-scale results. Two examples are the SRTM mission and the more recent TANDEM-X [3]. While these DEMs meet the requirements of a wide community of users, they pave the road for better DEM with finer planimetric and altimetric resolutions. Particularly, he high resolutions that become available allow to think to applications related to disaster management in urban areas. For these applications, the DEM is used to assess the damages occured to the buildings and to the man-made objects after e.g. an earthquake. Such applications require to be able to distinguish between neighbor buildings and to be able to count their floors. This is in line with the trend that considers the DEMs for SAR as a final product, compared to the one that considers them more as support products (for example for interferogram flattening in DInSAR). The generation of such DEMs is nowadays made possible by the higher bandwidth available for civil applications. However, the finer resolution results in smaller swaths and at the same time in more stringent requirements of geometry calibration. Thus, even if coarse resolution DEMs are exploited for calibration, the precise estimation of normal baselines becomes a challenge. In the next sections, we consider the case of single-pass spaceborne SAR interferometer, like a constellation or a single satellite with boom. The paper is focused on the main limits to the performances of the DEM, measured in terms of horizontal resolution and vertical accuracy. A mathematical model is developed to assess the accuracy of the location in 3D, given the two SAR images and a set of calibrated references. The mathematical model expresses the final accuracy as the combination of:

- the noise on the interferometric phases
- the accuracy of the GCP
- the contribution of images coregistration.

In the case of single pass interferometry, the phase error coming from thermal noise is the unavoidable term leading to the lower bound in the altimetric quality. This in turns leads to requirements to the system performance such as bandwidth, ambiguity rejection and the noise equivalent sigma zero. Volume decorrelation can be reduced by getting fine resolution cell, and minimizing penetration (say X band or higher). However, the error introduced by the limited knowledge of the interferometric baselines, can be hardly handled at system level (i.e. by imposing tight requirements to the boom stability). In fact, the normal baseline should be known with accuracy from millimiter to tens of micron, the most critical case being the boom configuration. Moreover this estimate should be enough frequent than the the dynamic of the boom itself.

The starting point that indicates that the interferometric baseline has to be known with micrometric accuracy, is derived through simple relations and, later, the performances of a novel calibration method, the 'split-swath', are derived. The main point of interest is the number of GCP needed to obtain the desired accuracy. With the limited swath size that can be obtained at low wavelengths,

Proc. 'Fringe 2011 Workshop', Frascati, Italy,
19–23 September 2011 (ESA SP-697, January 2012)

this is related also to the azimuth length of the calibration. It is found that, through the exploitation of the distance between the two split swaths, this calibration technique can reach micrometric accuracy in few seconds of acquisition. The advantage is to avoid complex evolution models for the baseline allowing a simple two-parameters calibration.

Finally, section 5.1 gives a numerical example considering a single-pass interferometer in Ka-band, with the objective of generating a DEM with 4 by 4 meters horizontal resolution and a vertical accuracy better than 1 m.

2. INTERFEROMETRIC MODEL

In this section we start from the interferometric equations and introduce simplifications to obtain simplified expressions that allow to write the DEM retrieval performances in a straightforward way.

2.1. The Interferometric equation

The absolute (unwrapped) data phase is modeled as superposition of signal and noise

$$\Phi_1(P) = -\tfrac{2\pi}{c} f_0 \left|\mathbf{R}_1(P)\right| + w_1(P) \quad (1)$$
$$\Phi_2(P) = -\tfrac{2\pi}{c} f_0 \left|\mathbf{R}_2(P)\right| + w_2(P) \quad (2)$$

In the monostatic case:

$$R_1(P) = |\mathbf{S_1}(\tau_1) - \mathbf{P}| + |\mathbf{S}_1(\tau_1 + \Delta\tau) - \mathbf{P}| \quad (3)$$
$$R_2(P) = |\mathbf{S_2}(\tau_2) - \mathbf{P}| + |\mathbf{S}_2(\tau_2 + \Delta\tau) - \mathbf{P}| \quad (4)$$

where $\Delta\tau$ is the (bistatic) lag between transmit and receive, $S_1(\tau)$ and $S_2(\tau)$ are the vectors that define the master and slave antenna center of phase. As these antennas are on the same body, connected to a boom, it is possible to model their trajectories as the center of mass of the satellite + mechanical and attitude variations. In the bistatic case:

$$R_1(P) = |\mathbf{S_1}(\tau_1) - \mathbf{P}| + |\mathbf{S}_1(\tau_1 + \Delta\tau) - \mathbf{P}| \quad (5)$$
$$R_2(P) = |\mathbf{S_1}(\tau_2) - \mathbf{P}| + |\mathbf{S}_2(\tau_2 + \Delta\tau) - \mathbf{P}| \quad (6)$$

The phase of the interferogram is:

$$\begin{aligned}\Phi_I &= \Phi_1(P) - \Phi_2(P) \\ &= -\frac{2\pi}{c} f_0 \left|\mathbf{R}_1(P)\right| + w_1(P) + \\ &\quad -\frac{2\pi}{c} f_0 \left|\mathbf{R}_2(P)\right| - w_2(P) \\ &= k_r \left(\left|\mathbf{R}_1(P)\right| - \left|\mathbf{R}_2(P)\right|\right) + w_\phi(P) \quad (7)\end{aligned}$$

where:

$$k_r = -\frac{2\pi}{c} f_0 \quad (8)$$
$$w_\phi(P) = w_1(P) - w_2(P) \quad (9)$$

2.2. Phase noise characterization

The total phase noise is a superposition of many effects, either due to additive noise sources, or to decorrelation of the two signals. The following noise sources adds up to both complex signals:

- thermal,
- quantization,
- ambiguities, from terrain and meteors (rain, ice, etc.),
- clutter from meteors.

Further decorrelation sources to be accounted for are:

- processing errors (including coregistration),
- defocusing due to boom jitter, APS variation in the integration time
- scene change (in the monostatic case only, but very small)
- volumetric decorrelation
- azimuth common-band decorrelation (introduced by non-aligned Doppler).

Furthermore we model the source as a distributed target, or fully developed speckle, i.e. a circular Normal, zero mean. The amplitude fluctuations cause bad performances in the interferometric phase estimation, unless the interferogram is prior averaged on - say N_L >4 looks [1]. Under this assumption, we expect that the Signal to Phase Noise in the Multi Look averaged interferogram is large, that is necessary for a proper phase unwrapping. Unwrapping error will not be accounted for here. When the number of looks is large, the variance of the phase is related to the coherence by the Cramer Rao Bound (see [2] for a review of statistics in interferometry):

$$\sigma_\phi^2 \geq \sigma_{CRB}^2 = \frac{1-\gamma^2}{2\gamma^2 R} = \frac{1-\gamma^2}{2\gamma^2 N_L} \quad (10)$$

The coherence is computed by combining all the contributions from the different decorrelation sources as follows:

$$\gamma = \gamma_{th} \times \gamma_v \ldots \times \gamma_N \quad (11)$$

where the product is to be extended to all the decorrelation sources. The expression for each γ can be found in [3].

3. LOCATION EQUATIONS IN 3D

The interferometric equation (7) expresses a relation between the unknown target location $P(x_p, y_p, z_p)$ and the antenna's phase centre $S_n(x_s(\tau), y_s(\tau), z_s(\tau))$ (where n=1 and 2), that is known with errors, to be calibrated. In a local scale (small variation of τ), we may assume a linear model: $\mathbf{S}_n(\tau) = \mathbf{S}_{0n}(\tau_0) + \mathbf{v}_n(\tau - \tau_0)$ Even in the case where the trajectory of the antennas are known, one equation is not enough for three unknowns, and we have to add range and Doppler equations. The range equation, for the master reference is: $|\mathbf{S}_1(\tau) - \mathbf{P}| + |\mathbf{S}_1(\tau + \Delta\tau) - \mathbf{P}| = ct_b$ where t_b is the overall travel time (two-way, accounting for transmit and receive), that is the range coordinate in the Slant Range, Doppler reference of the focused dataset. The Doppler equation for the target at azimuth coordinate τ, and acquisition Doppler centroid f_D is:

$$f_D = \frac{1}{2\pi}\frac{\partial\phi_1}{\partial\tau} = -\frac{f_0}{c}\frac{\partial(R_1(\tau) + R_2(\tau + \Delta\tau))}{\partial\tau} \quad (12)$$

In principle there are two different Doppler equations for Master and Slave, but this effect is ignored, in fact the Doppler shift should be much smaller than the Doppler bandwidth (to avoid decorrelation due to non-common band).

So far, we have three equations in three unknowns:

- The range equation

$$\frac{|\mathbf{S}_1(\tau) - \mathbf{P}| + |\mathbf{S}_1(\tau + \Delta\tau) - \mathbf{P}|}{c} = t \quad (13)$$

- The Doppler equation:

$$-\frac{2}{\lambda}\frac{\partial(R_1(\tau) + R_2(\tau + \Delta\tau))}{\partial\tau} = -\frac{2v}{\lambda}\sin\psi = f_D \quad (14)$$

- The interferometric equation:

$$k_r\left(|\mathbf{R}_1(P)| - |\mathbf{R}_2(P)|\right) = \psi \quad (15)$$

where $t, f_{D,}\psi$ are random variables expressing the noisy measures of range, Doppler frequency and interferometric phase. However, in presence of uncertainties of the antenna trajectories, we have to add further unknown terms. For the sake of performance evaluation, we can introduce several assumptions, that do not hold if the estimation (say the inversion of the three equations) is the goal. First , we ignore the bistatic delay, between transmit and receive. The difference between the bistatic and the two-way monostatic:

$$\begin{aligned}\Delta r_b &= 2\left(\sqrt{r_0^2 + v_s^2\left(\tfrac{r_0}{c}\right)^2} - r_0\right)\\ &\simeq 2r_0\tfrac{v_s^2}{c^2}\end{aligned}$$

is a really small fraction of the slant range. This can be properly compensated in focusing data. Assuming:

- small errors, so that we can linearize the functions in correspondence of the optimum.
- monostatic system (the extension to the bistatic being possible)
- zero-Doppler (broadside pointing) , as this gives to the maximum geometric and radiometric sensitivity.

This last assumption simplifies the Doppler Equation, as Zero Doppler is orthogonal with orbit, hence is we assume *x axis oriented along track* and parallel to ground, and for large sensor-target distance, *r*:

$$\begin{aligned}-\frac{2v}{\lambda}\sin\psi &\simeq -\frac{2v}{\lambda}\psi \simeq -\frac{2v}{\lambda}\frac{x - x_s}{r}\\ x - x_s &\simeq x_a\end{aligned}$$

x_s being the sensor position, x the target's one, and x_a is the observable, i.e. the measure of the target location in the slant range, zero Doppler plane. We can then summarize the location equations by converting times into distances:

- Doppler Equation

$$\begin{aligned}x - x_s &\simeq x_a\\ x_a &\sim N(x, \sigma_a)\end{aligned} \quad (16)$$

where σ_a is the azimuth resolution,

- Master range equation

$$\begin{aligned}|\mathbf{S}_1(\tau_1) - \mathbf{P}|^2 =\\ (x_P - x_{S1}(\tau_1))^2 + (y_P - y_{S1}(\tau_1))^2 +\\ (z_P - z_{S1}(\tau_1))^2 = r^2\end{aligned} \quad (17)$$

where:

$$r \sim N\left(r_p = \frac{ct_p}{2}, \sigma_r\right) \quad (18)$$

where r is the range of the target in P, measured with an error may assume zero-mean, normal distributed, σ_r is the standard deviation in the target location.

- Interferometric equation

$$|\mathbf{S}_1(\tau_1) - \mathbf{P}| - |\mathbf{S}_2(\tau_2) - \mathbf{P}| = -\frac{\Phi}{2\pi}\lambda \quad (19)$$

where Φ is the unwrapped phase $\Phi \sim N(\Phi_p, \sigma_\phi)$.

3.1. Single pass interferometry case

Considering the case of system able to acquire two simultaneous observations by two antennas connected by a boom, the interest is to evaluate the location accuracy in both planimetry and altimetry. As a consequence, we select a target of interest, P, and chose the local reference system, tangent to the earth in P as shown in figure 1:

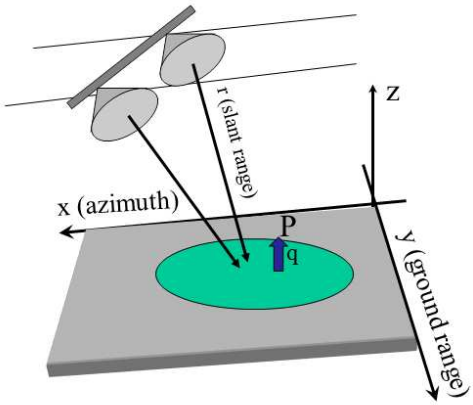

Figure 1. Interferometer geometry and local reference systems.

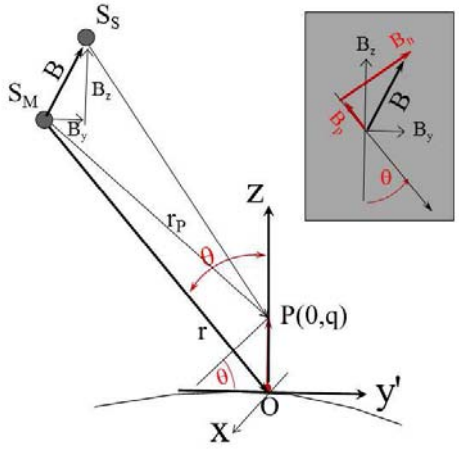

Figure 2. Interferometer geometry and local reference systems.

- the x-axis spans the horizontal plane directed along track, thus it is azimuth,
- the y-axis spans the horizontal plane directed across track, thus it is ground range,
- the z-axis is vertical.

In figure 2 we put the reference in O, and the target in the specific location P(x_p=0,y_p=0,q). Considering Zero-Doppler pointing, the location equations are:

$$\begin{aligned} f_1(\mathbf{x}_g) &= x \\ f_2(\mathbf{x}_g) &= |\mathbf{S}_M - \mathbf{P}| = r \\ f_3(\mathbf{x}_g) &= |\mathbf{S}_M - \mathbf{P}| - |\mathbf{S}_S - \mathbf{P}| = \frac{\Phi}{2\pi}\lambda \end{aligned} \quad (20)$$

where $r \sim N\left(r_p = \frac{ct_p}{2}, \sigma_r\right)$, $\Phi \sim N(\Phi_p, \sigma_\psi)$ and $x \sim N(x_p, \sigma_a)$.

Sensors, target and baseline In order to evaluate these equations, we assume the locations of satellites and target in the local reference as follows:

$$S_M = [\ 0 \quad -r\sin\theta \quad r\cos\theta\ ]^T \quad (21)$$

$$S_S = [\ 0 \quad -r\sin\theta + B_y \quad r\cos\theta + B_z\ ]^T \quad (22)$$

$$P = [\ x_p \quad y_P \quad q\ ]^T \quad (23)$$

In such system, the location equations can be entirely evaluated in the zero-Doppler plane orthogonal to the orbit, hence to azimuth direction. The component of the interferometer baseline out this plane, is responsible only of an azimuth shift provided that the two images are filtered with in the same common bandwidth centered on Doppler zero. The azimuth shift can be ignored, as it is estimated by coregistration and compensated. Therefore, the baseline is entirely characterized by either the (x,z) or (normal, parallel) components (see figure 2).

$$\begin{bmatrix} B_n \\ B_p \end{bmatrix} = \begin{bmatrix} \cos\theta & \sin\theta \\ -\sin\theta & \cos\theta \end{bmatrix} \begin{bmatrix} B_y \\ B_z \end{bmatrix}$$

By plugging into (20), after linearization and with the coordinate change of variable :

$$\begin{aligned} y' &= y_p - \tfrac{q}{\tan\theta} \\ y_p &= y' + \tfrac{q}{\tan\theta} \end{aligned}$$

we obtain:

$$\begin{aligned} x &= x_p \\ r + y'_p \sin\theta &= r_p \\ \frac{B_n}{r}\frac{q}{\sin\theta} + y'_p\frac{B_n}{r}\cos\theta - y'_p\frac{B_p\sin\theta}{r} - B_p &\simeq \frac{\lambda}{4\pi}\phi \end{aligned} \quad (24)$$

where the first term in (24) is the topographic-dependent phase, the sole useful for DEM generation, the second and third are due to displacement of target with respect to its nominal position, that nulls for $y'_p = 0$ and the last is just the slant range shift of the second image, B_p. All these these three terms can be made small in the interferogram co-registrat ion and are usually ignored.

4. MODEL FOR LOCATION ACCURACY EVALUATION

Let us express the vector of the unknown target position: $\mathbf{x} = [\ x_P \quad y_P \quad z_P\ ]^T$ the vector of the measures, that are stochastic processes, so far assumed Normal distributed: $\mathbf{y} = [\ t \quad \tau \quad \psi\ ]^T$ and the non linear functions:

$$\mathbf{f}(\mathbf{x}) = \begin{bmatrix} f_1(\mathbf{x},\mathbf{q}) \\ f_2(\mathbf{x},\mathbf{q}) \\ f_3(\mathbf{x},\mathbf{q}) \end{bmatrix} =$$

$$= \begin{bmatrix} x \\ |\mathbf{S}_1(\tau_1,\mathbf{q}) - \mathbf{p}| \\ |\mathbf{S}_1(\tau_1,\mathbf{q}) - \mathbf{p}| - |\mathbf{S}_2(\tau_2,\mathbf{q}) - \mathbf{p}| \end{bmatrix} = \mathbf{d} \quad (25)$$

where $\mathbf{d} = \begin{bmatrix} x_a \\ r \\ \frac{\psi}{2\pi}\lambda \end{bmatrix}$ and we have explicated the dependence of the satellite position with respect to the track by introducing a vector of unknown parameters, $\mathbf{q}$ of size $[N_\theta, 1]$. The parameters are those necessary to locate the two center of phases in the 3D space, for each time.

4.1. Standard deviation of the location error

We can linearize the system near the optimal solution, the exact location of the target, $\mathbf{x} = \mathbf{x}_0$, and the exact value of the baseline parameters, $\mathbf{q} = \mathbf{q}_0$. The total differential of the measurable is:

$$\begin{aligned} \boldsymbol{\Delta}_d &= \frac{\partial \mathbf{f}}{\partial \mathbf{x}}\Big|_{\mathbf{x}=\mathbf{x}_0} \boldsymbol{\Delta}_x + \frac{\partial \mathbf{f}}{\partial \mathbf{q}}\Big|_{q=q_0} \boldsymbol{\Delta}_\theta \\ \boldsymbol{\Delta}_d &= \mathbf{J}_x \boldsymbol{\Delta}_x + \mathbf{J}_q \boldsymbol{\Delta}_q \end{aligned} \tag{26}$$

where $\mathbf{J}_x$ is the [3,3] Jacobean obtained by differentiating the three equations versus each of the three target coordinates: $\mathbf{J} = \{J_{ij}\} = \left\{\frac{\partial f_i}{\partial x_j}\right\}$ and $\mathbf{J}_q$ is the $[3, N_q]$ is Jacobean obtained by differentiating of the N_q "baseline parameters". Notice that the estimates error, $\boldsymbol{\Delta}_x$, is zero-mean and as $\boldsymbol{\Delta}_\theta$ is zero mean (that is, we assume that the reference DEM is unbiased, as for the SRTM [9]). In this case, the target location is unbiased. The covariance of the estimates:

$$\mathbf{C}_{\boldsymbol{\Delta}_x} = E\left[\boldsymbol{\Delta}_x \boldsymbol{\Delta}_x^T\right] = E\left[\boldsymbol{\Delta}_x \boldsymbol{\Delta}_x^T\right] = \begin{bmatrix} \sigma_{x_P}^2 & E[x_P y_P] & E[x_P z_P] \\ E[x_P y_P] & \sigma_{y_P}^2 & E[y_P z_P] \\ E[x_P z_P] & E[y_P z_P] & \sigma_{z_P}^2 \end{bmatrix} \tag{27}$$

has on its diagonal the variances of the location error in the 3D. In order to compute $\mathbf{C}_{\boldsymbol{\Delta}_x}$, we have to invert the 3-by-3 equation system 25, that we expect to be well conditioned (otherwise, location solution would be impossible), therefore:

$$\begin{aligned} \boldsymbol{\Delta}_d - \mathbf{J}_q \boldsymbol{\Delta}_q &= \boldsymbol{\Delta}_x \\ \boldsymbol{\Delta}_x &= \mathbf{J}_x^{-1}\left(\boldsymbol{\Delta}_d - \mathbf{J}_q \boldsymbol{\Delta}_q\right) \end{aligned} \tag{28}$$

and from this we derive the covariance

$$\begin{aligned} \mathbf{C}_{\boldsymbol{\Delta}_x} &= E\left[\boldsymbol{\Delta}_x \boldsymbol{\Delta}_x^T\right] = \\ &= \mathbf{J}_x^{-1} \mathbf{C}_{\boldsymbol{\Delta}_d} \left(\mathbf{J}_x^{-1}\right)^T + \mathbf{J}_x^{-1} \mathbf{J}_q \mathbf{C}_{\boldsymbol{\Delta}_q} \mathbf{J}_q^T \left(\mathbf{J}_x^{-1}\right)^T \end{aligned} \tag{29}$$

that has been derived by assuming incorrelation between the estimate of the orbit and the data *d*. According to 29, the error is the superposition of two contributions:

- the first term expresses the contribution of the three measures (the range, the phase and the Doppler), and corresponds to the location accuracy when the geometry is perfectly known
- the second term is the contribution of the unknown geometry, to be calibrated for.

Calibration by reference GCP In order to estimate the location of master and slave, we assume that a suitable set of Ground Control Points are given, say N_g geometrically calibrated targets. These may come from a SRTM DEM, or we may assume a reference surface, like the sea-level. In principle, we should select $N_g \geq N_q$, and we expect that the number of target is in excess with respect the unknown orbit parameters particularly if the accuracy of the GCP is bad.

For the sake of local accuracy evaluation, we can still assume a linear system, but now we have much more observations. We handle this by stacking many equations like 25 one upon another, up to $N_g \times 3$ equations:

$$\mathbf{f}_g(\mathbf{x}) = \begin{bmatrix} \mathbf{f}(\mathbf{x}_g(1), \mathbf{q}) \\ \dots \\ \mathbf{f}(\mathbf{x}_g(N_g), \mathbf{q}) \end{bmatrix} = \mathbf{d}_g \tag{30}$$

$$\mathbf{d}_g = \begin{bmatrix} \mathbf{d}(1) \\ \dots \\ \mathbf{d}(N_g) \end{bmatrix} \tag{31}$$

The total differential:

$$\boldsymbol{\Delta}_{dg} = \mathbf{J}_{xg} \boldsymbol{\Delta}_{xg} + \mathbf{J}_{qg} \boldsymbol{\Delta}_q$$

is an overdetermined system of equations that can be solved in Least Square for the unknowns:

$$\begin{aligned} \boldsymbol{\Delta}_{dg} - \mathbf{J}_{xg} \boldsymbol{\Delta}_{xg} &= \mathbf{J}_{qg} \boldsymbol{\Delta}_q \\ \boldsymbol{\Delta}_\theta &= \mathbf{J}_{qg}^\dagger \left(\boldsymbol{\Delta}_{dg} - \mathbf{J}_{xg} \boldsymbol{\Delta}_{xg}\right) \\ \mathbf{J}_{\theta g}^\dagger &= \left(\mathbf{J}_{qg}^T \mathbf{J}_{qg}\right)^{-1} \mathbf{J}_{qg}^T \end{aligned} \tag{32}$$

where the symbol "†" stands for pseudo-inversion. Equation 32 can now be exploited for evaluating the covariance of the estimates of track parameters $\mathbf{C}_{\boldsymbol{\Delta}_\theta} = \mathbf{J}_{qg}^\dagger \mathbf{C}_{\boldsymbol{\Delta}_{dg}} \mathbf{J}_{qg}^\dagger + \mathbf{J}_{qg}^\dagger \mathbf{J}_{xg} \mathbf{C}_{\boldsymbol{\Delta}_{xg}} \mathbf{J}_{xg}^T \mathbf{J}_{qg}^\dagger$ where $\mathbf{C}_{\boldsymbol{\Delta}_{xg}}$ is the covariance of the location of the ground control points. This equation is to be replaced into the second term of 25 to provide the required accuracy:

$$\begin{aligned} \mathbf{C}_{\boldsymbol{\Delta}_x} = \mathbf{J}_x^{-1} \mathbf{C}_{\boldsymbol{\Delta}_d} \left(\mathbf{J}_x^{-1}\right)^T + \mathbf{J}_x^{-1} \mathbf{J}_q \mathbf{J}_{qg}^\dagger \mathbf{C}_{\boldsymbol{\Delta}_{dg}} \mathbf{J}_{qg}^\dagger \mathbf{J}_q^T \left(\mathbf{J}_x^{-1}\right)^T \\ + \mathbf{J}_x^{-1} \mathbf{J}_q \mathbf{J}_{qg}^\dagger \mathbf{J}_{xg} \mathbf{C}_{\boldsymbol{\Delta}_{xg}} \mathbf{J}_{xg}^T \mathbf{J}_{qg}^\dagger \mathbf{J}_q^T \left(\mathbf{J}_x^{-1}\right)^T \end{aligned} \tag{33}$$

The interpretation of this expression is straightforward, as the total location error on each target is the summation of three errors:

- the location error in case of perfect knowledge of the geometry;
- the contribution of the intrinsic error of the reference DEM (or GCP)
- the error due to the location of the GCP in the SAR image.

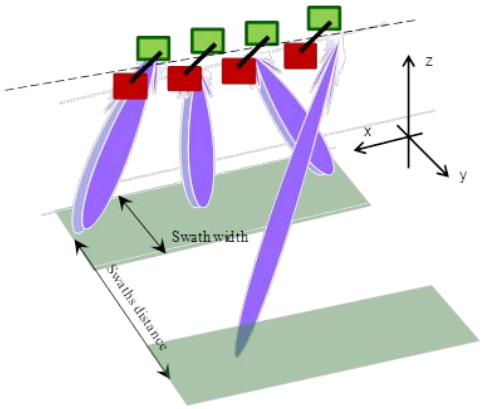

Figure 3. Schematic representation of the split-swath acquisition geometry with TOPSAR mode.

Notice that the pseudoinversion of the Jacobean $\mathbf{J}_{\theta g}^{\dagger}$ has the fundamental role of nulling this last two contributions, that is the desired result, leaving the sole unavoidable first one. In order to get that goal, we notice how using many coarse GCPs is quite better than few 'good' ones.

5. NORMAL AND PARALLEL BASELINE ESTIMATION ACCURACY FROM GCPS

In this section we analyze a possible real situation to evaluate the accuracy of the estimation of the normal and the parallel component of the baseline. Let us assume the general case of N_g GCPs uniformly spaced in ground range, that applies if we use SRTM or any other reference DEM and, for simplicity, zero elevation. Under these assumptions, a system of N_g equations with two unknowns comes out:

$$\mathbf{A} = \begin{bmatrix} 0 & -1 \\ d \cdot \cos(\theta)/r & -(d/r) \cdot \sin(\theta) - 1 \\ (N_g - 1) \cdot d \cdot \left(\frac{\cos(\theta)}{r}\right) & -(N_g - 1)\frac{d}{r}\frac{\sin(\theta)}{r} - 1 \end{bmatrix}$$

$$\mathbf{B} = \begin{bmatrix} B_n \\ B_p \end{bmatrix} \tag{34}$$

$$\mathbf{AB} = \frac{\lambda}{4\pi}\phi \tag{35}$$

The solution of the system above is straightforward with the pseudoinverse and the Least Square technique, and the covariance is:

$$E\left[BB^T\right] = \left(A^T A\right)^{-1}\left(\frac{\lambda}{4\pi}\sigma_\phi\right)^2 \tag{36}$$

Introducing the following substitutions:

$$m = \frac{d}{r}\cos(\theta) \qquad p = tan(\theta) \tag{37}$$

$$k = \frac{\lambda}{4\pi} \qquad z = \frac{3}{N_g} \cdot k^2\sigma_\phi^2 \tag{38}$$

$$a = m^2p^2\left(2N_g^2 - 3N_g + 1+\right) \tag{39}$$

the accuracy of the normal and parallel baseline after calibration result:

$$\sigma_{B_n}^2 = \frac{a + 4mp\left(N_g - 1\right) + 6}{m^2\left(4N_g^2 - 5N_g + 1\right)} \cdot z \tag{40}$$

$$\sigma_{B_p}^2 = \frac{3\left(2N_g - 1\right)}{N_g\left(4N_g - 1\right)}\left(k \cdot \sigma_\phi\right)^2 \simeq \frac{1}{N_g}\frac{3}{2}\left(k \cdot \sigma_\phi^2\right)^2 \tag{41}$$

The dependence of the normal baseline accuracy on the inverse of the total DEM extent in ground range suggests for the split swath configuration shown in Fig 5. As a matter of fact, if the swath width is negligible with respect to the distance between the two swaths, the accuracy on the normal baseline turns out to be leaded by the following term:

$$\sigma_{B_n}^2 = \frac{3}{N_r}\frac{2p^2N_r^2 - 3p^2N_r + p^2}{4N_r^2 - 5N_r + 1}k^2\sigma_\phi^2 \tag{42}$$

i.e. the contiguous swath solution is expected to give performances worse than or equal to the novel split swath solution.

5.1. Numeric example in the Ka-band case

The accuracy of the estimation depends on an unavoidable term bound to the quality (i.e.: the coherence γ and the ENL) of the interferogram. This remains the main driver in defining the requirements for the instrument. On top of this, the accuracy on the estimation of the centre of phase position (i.e.: the baseline and its normal and parallel components) are calibrable terms, as derived in previous section. Fig.4 reports the results of numerical performance evaluation for the case of Ka-band sensor ($\lambda = 8mm$) with a boom of 22m. On the top figure the error on DEM retrieval is plotted versus the number of looks for different values of coherence. On the bottom figure, the vertical accuracy is reported against the baseline accuracy.

Considering a SRTM reference DEM, with an accuracy of 5m, Fig. 5 represents the accuracy of the parallel and normal baseline components as a function of the acquisition duration for different swaths' width. The case of continuous swaths is compared to the novel split swath technique. (The distance between swaths is assumed to be 75 km). No difference comes out for the parallel baseline component, while the better results of the split-swath technique are evident on the normal baseline case. The error smaller than 10 micron is reached with a very short acquisition (in the order of 2 km) by the split swath technique whilst the contiguous swath method needs at least a double duration of the acquisition thus leading to more constraining requirements on the satellite structure (e.g.:

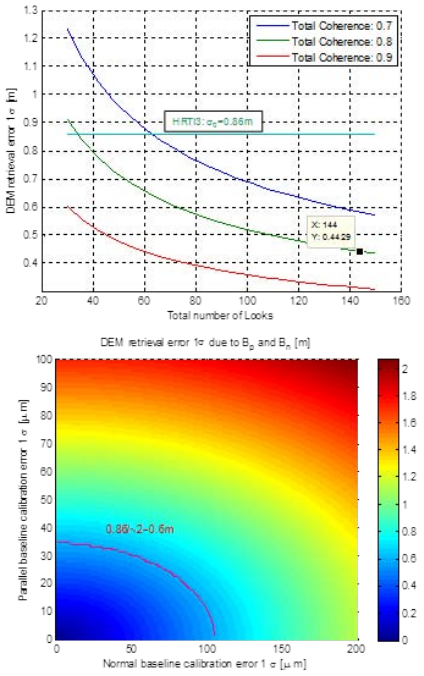

Figure 4. Top: the error on DEM retrieval due to signal; bottom: the contribution to the DEM error caused by baseline accuracy.

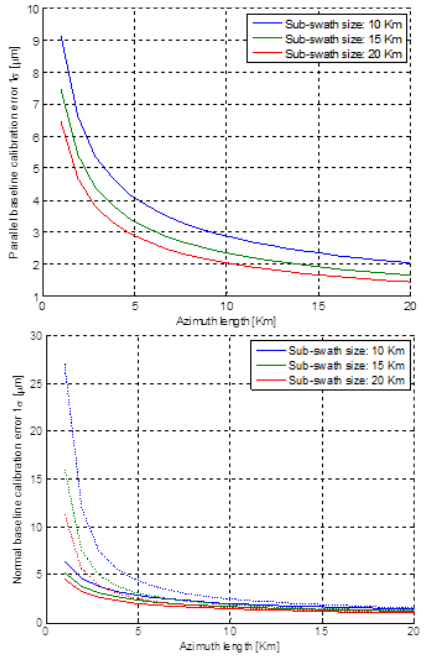

Figure 5. Top: the error on the parallel baseline versus the acquisition length for different swaths; bottom: error on the normal baseline versus the acquisition length for different size of the swath. The dashed line refers to the continuous swath technique whilst the solid line accounts for the novel split-swaths technique.

Table 1. Sample DEM performance in Ka-band.

Parameters	HRTI+	HRTI++
SNCR [dB]	30	30
SNR [dB]	12	16
ASR [dB]	-17	-17
SQNR [dB]	20	20
Resolution (Sl.Rg. x Az.)[m2]	0.30 x 2	0.30 x 1
Input DEM res. [m2]	90 x 90	90 x 90
Input DEM accuracy [m]	5	5
Cal. length [km]	2	5
Swath width [km]	10	9
Swath distance [km]	75	75
Total coherence	0.91	0.94
ENL	29.89	18
Output DEM res. [m2]	6 x 6	4 x 4
Output DEM accuracy [m]	0.65	0.74

boom vibration). These results are valid also for very narrow swaths (e.g.: 10 km).

Tab. 1 resumes the vertical accuracy that can be achieved for two cases: a 6x6 m and a 4x4 m resolution DEMs. It can be noted that the driver for the performances is the SNR ratio, that strongly affects the coherence required to be better than 0.9. The calibration is performed on a 10 km width swath with a 2 km long acquisition that corresponds to less than a second of acquisition.

REFERENCES

[1] A Ferretti, A Monti Guarnieri, C. Prati, F. Rocca, and D. Massonnet. InSAR Principles: Guidelines for SAR Interferometry Processing and In- terpretation. ESA, esa tm-19 feb 2007 edition, 2007.

[2] Richard Bamler and Philipp Hartl. Synthetic aperture radar interferometry. Inverse Problems, 14:R1-R54, 1998.

[3] G. Krieger, A. Moreira, H. Fiedler, Hajnsek, M. I. Zink, and M. Werner. TanDEM-X: A satellite formation for high-resolution SAR interferometry. In Fourth International Workshop on ERS/Envisat SAR Interferometry, 'FRINGE05', Frascati, Italy, 28 Nov-2 Dec 2005, pages 1-7, December 2005.

[4] Fabio Gatelli, Andrea Monti Guarnieri, Francesco Parizzi, Paolo Pasquali, Claudio Prati, and Fabio Rocca. The wavenumber shift in SAR interferometry. IEEE Transactions on Geoscience and Remote Sensing, 32(4):855-865, July 1994.

[5] D. Moller, S. Hensley, G.A. Sadowy, C.D. Fisher, T. Michel, M. Zawadzki, and E. Rignot. The

glacier and land ice surface topography interferometer: An airborne proof-of-concept demonstration of high-precision ka-band single-pass elevation mapping. Geoscience and Remote Sensing, IEEE Transactions on, 49(2):827-842, feb. 2011.

[6] K.P. Papathanassiou and S.R. Cloude. Single-baseline polarimetric sar interferometry. Geoscience and Remote Sensing, IEEE Transactions on, 39(11):2352 2363, nov 2001.

[7] J.H. Gonzalez, M. Bachmann, G. Krieger, and H. Fiedler. Development of the tandem-x calibration concept: Analysis of systematic errors. Geoscience and Remote Sensing, IEEE Transactions on, 48(2):716-726, 2010.

[8] E. Sansosti. A simple and exact solution for the interferometric and stereo sar geolocation problem. Geoscience and Remote Sensing, IEEE Transac- tions on, 42(8):1625-1634, August 2004.

[9] A. Koch and C. Heipke. Quality assessment of digital surface models derived from the shuttle radar topography mission (srtm). In Geoscience and Remote Sensing Symposium, 2001. IGARSS '01. IEEE 2001 International, 2001.

[10] Bernhard Rabus, Michael Eineder, Achim Roth, and Richard Bamler. The shuttle radar topography mission-a new class of digital elevation models acquired by spaceborne radar. ISPRS Journal of Photogrammetry and Remote Sensing, 57(4):241-262, 2003.

[11] V.M. Enjolras and E. Rodriguez. An assessment of a ka-band radar interferometer mission accuracy over eurasian rivers. Geoscience and Remote Sensing, IEEE Transactions on, 47(6):1752-1765, june 2009.

[12] R. Bamler and M. Eineder. Split band interferometry versus absolute ranging with wideband sar systems. In Geoscience and Remote Sensing Symposium, 2004. IGARSS '04. Proceedings. 2004 IEEE International, volume 2, pages 980-984 vol.2, 2004.